Multichannel *R*-matrix analysis of elastic and inelastic resonances in the ^{21}Na + *p* compound system

C. Ruiz,* T. Davinson, F. Sarazin,† I. Roberts, A. Robinson, and P. J. Woods
University of Edinburgh, Edinburgh, EH9 3JZ, UK

L. Buchmann, A. C. Shotter, and P. Walden
TRIUMF, Vancouver, BC V6T 2A3, Canada

N. M. Clarke
University of Birmingham, Birmingham B15 2TT, UK

A. A. Chen‡
Simon Fraser University, Burnaby, BC V5A 1S6, Canada

B. R. Fulton, D. Groombridge, and J. Pearson‡
University of York, York YO10 5DD, UK

A. S. Murphy§
Ohio State University, Columbus, Ohio, USA
(Received 25 October 2004; published 15 February 2005)

A multichannel *R*-matrix formalism was used to fit ^{21}Na + *p* resonant elastic and inelastic scattering data taken at the TRIUMF UK detector array facility at TRIUMF-ISAC. Five resonances were observed corresponding to states in ^{22}Mg above the proton threshold. Four of these corresponded to states seen in previous transfer reaction studies where firm spin-parity assignments could not be made. One new resonance, previously unobserved in any reaction, was also seen. Where possible, resonance energies, partial widths, and spin-parity values of these resonances were extracted. The correspondence between these states and possible analogs in the mirror nucleus ^{22}Ne is discussed, as well as the relation to $T = 1$ states in the nucleus ^{22}Na.

DOI: 10.1103/PhysRevC.71.025802 PACS number(s): 25.60.Bx, 25.40.Ny, 21.10.−k

I. INTRODUCTION

The structure of the radionuclide ^{22}Mg has received much attention in recent years by both experimentalists and theorists because of its role in determining the properties of astrophysical reaction rates relating to the production of ^{22}Na in explosive stellar scenarios.

The nuclide ^{22}Na β decays with a half-life of 2.6 years with the emission of a characteristic γ ray of energy 1.275 MeV. This makes it an important observable in the quest to understand nucleosynthesis along the proton-rich side of stability around the NeNa cycles, in classical novae, x-ray bursters, and type 1a supernovae. ^{22}Na is primarily formed in hot hydrogen-rich environments via the reaction ^{21}Ne(p, γ)^{22}Na, the stable ^{21}Ne being the result of β-decay of ^{21}Na. As temperatures rise, the formation of ^{22}Mg via the reaction ^{21}Na(p, γ)^{22}Mg is facilitated by resonances in the ^{21}Na + *p* system dependent on the nuclear properties of states in ^{22}Mg. This can lead to increased production of ^{22}Na in these hot environments since ^{22}Mg(p, γ)^{23}Al is slow; however, ^{22}Na may then be destroyed via further proton captures, the rate of which may also be enhanced at these temperatures. The net result is that the final abundance of ^{22}Na is delicately linked to the balance and interplay of the reaction network in this mass region, with certain reactions, including ^{21}Na(p, γ)^{22}Mg, playing a significant role.

Investigations with the Compton in γ-ray space telescope (COMPTEL) found no detected flux of 1.275 MeV γ rays above background from a survey of several ONe type novae [1]. Subsequent studies of fluxes from particular sources, including the classical slow CO white dwarf nova Casseopeiae 1995 and the ONe nova Velorum 1999, were able to place an upper limit on the amount of ^{22}Na in those sites based on marginal detection of the 1.275 MeV line [2]. It was thought that ONe novae were responsible for the synthesis of most of the ^{22}Na in the interstellar medium [3], and yet COMPTEL was unable to detect the flux predicted by contemporary nova models from candidate ONe novae. It is therefore still of vital interest that the models of nova nucleosynthesis be refined in order that future space-based observation, such as the INTEGRAL mission [4], has improved confidence in its identification of ^{22}Na-producing sites.

*Electronic address: ruiz@triumf.ca; also at Simon Fraser University, Burnaby, BC V5A 1S6, Canada; TRIUMF, Vancouver, BC V6T 2A3, Canada.

†Present address: Dept. of Physics, Colorado School of Mines, Golden, CO 80401, USA.

‡Present address: McMaster University, Hamilton, ON, Canada.

§Present address: University of Edinburgh, Edinburgh, EH9 3JZ, UK.

TABLE I. Excitation energies (keV) of ^{22}Mg states above the proton threshold, resulting from previous experimental studies. Values marked with an asterisk were used as calibration points in their respective experiments.

(p,t) [14]	(p,t) [8]	$(^3\mathrm{He},n)$ [9]	$(^3\mathrm{He},n)$ [11]	$(^3\mathrm{He},n\gamma)$ [10]	$(^3\mathrm{He},n\gamma)$ [22]	$(^{16}\mathrm{O},^6\mathrm{He})$ [19]	$(^3\mathrm{He},^6\mathrm{He})$ [17]	Average values[a]	J^π
5713.9*	5738 ± 35	5699 ± 20	5680 ± 30	5714.4 ± 1.5 5837 ± 5	5713 ± 2	5711 ± 13	5713.9*	5713.9 ± 1.2 5837 ± 5	2^+
5961.9 ± 2.5		5945 ± 20	5980 ± 30					5961.9 ± 2.5	0^+
6045.8 ± 3.0	6061 ± 37					6041 ± 11	6051 ± 4	6045.6 ± 2.9	(1^-)
6246.4 ± 5.1[b]	(6281 ± 33)[c]	6263 ± 20[c]	(6220 ± 50)[c]	(6298 ± 50)[c]		6255 ± 10	6246 ± 4	6248.2 ± 4.5[c]	$(4^+–6^+)$
6322.6 ± 6.0	(6281 ± 33)[c]		(6220 ± 50)[c]	(6298 ± 50)[c]			6329 ± 6	6322.6 ± 6.0	
6613 ± 7[d]	6645 ± 44	6573 ± 20				6606 ± 11	6616 ± 4	6608.5 ± 5.6	(2^+)
6787 ± 14	6836 ± 44	6770 ± 20	6760 ± 90			6767 ± 20	6771 ± 5	6780.4 ± 9.6	(3^-)
						6889 ± 10	6878 ± 9	6884 ± 13	

[a]Average values from Ref. [14].
[b]Probably a doublet [14].
[c]The states at $E_x = 6249$ and 6323 keV were not resolved by these measurements.
[d]Possibly a multiplet of states [14].

Of critical importance to the understanding of the production of ^{22}Na in these sites and the improvement of the models is the nuclear structure information about states in ^{22}Mg relating to the rate of the $^{21}\mathrm{Na}(p,\gamma)^{22}\mathrm{Mg}$ reaction. The final amount of ^{22}Na produced in the nova event in present hydrodynamic simulations containing reaction networks can vary by orders of magnitude given the degree of uncertainty present until recently in the values of the reaction rate (see for example, the work of Iliadis *et al.* [5] and Jose *et al.* [6], investigating the effect of these uncertainties on abundances in nova models).

In this study, data taken in an experiment at the TRIUMF UK detector array (TUDA) facility at TRIUMF-ISAC, previously reported in Ref. [7], are revisited through a superior analysis. The results presented here supersede those of Ref. [7].

II. PREVIOUS EXPERIMENTAL STUDIES

It is known that ^{22}Mg shows a strong two-particle structure and its levels are populated strongly in two-particle transfer reactions such as $^{24}\mathrm{Mg}(p,t)^{22}\mathrm{Mg}$ [8]. Prior to the recent astrophysics interest in ^{22}Mg, most of the structure had been mapped using the aforementioned reaction, other reactions such as $^{20}\mathrm{Ne}(^3\mathrm{He},n\gamma)^{22}\mathrm{Mg}$ [9–11], and β spectroscopy of ^{22}Al [12,13]. Recently, additional $^{24}\mathrm{Mg}(p,t)^{22}\mathrm{Mg}$ studies [14–16] have been undertaken as well as studies of such reactions as $^{25}\mathrm{Mg}(^3\mathrm{He},^6\mathrm{He})^{22}\mathrm{Mg}$ [17], $^{24}\mathrm{Mg}(^4\mathrm{He},^6\mathrm{He})^{22}\mathrm{Mg}$ [18], and $^{12}\mathrm{C}(^{16}\mathrm{O},^6\mathrm{He})^{22}\mathrm{Mg}$ [19]. The work of Bateman *et al.* [14] led to the identification of new astrophysically relevant states, which were corroborated by Refs. [17–19]. The work of Refs. [15,16] attempted to assign spin parities to some of the astrophysically important levels.

Table I summarizes the experimental knowledge of astrophysically relevant states in ^{22}Mg prior to this experiment. The proton threshold in ^{22}Mg was previously thought to be 5.502 MeV; however, recent measurements of resonance energies in $^{21}\mathrm{Na} + p$ using the DRAGON recoil separator at TRIUMF-ISAC implied that the previously accepted mass of ^{22}Mg was incorrect by 6 keV [20]. A reanalysis of one of the experiments that measured the ^{22}Mg mass produced results consistent with this observation [21]. As a result, the value of the proton threshold in ^{22}Mg used in this work is 5.508 MeV.

III. EXPERIMENTAL SETUP

This study was performed using the first accelerated radioactive beam at TRIUMF-ISAC [23] and the TUDA facility located there. The ^{21}Na ions with typical intensities of 5×10^7 ions/s were used, although one order of magnitude greater intensity was available. The intensity used was limited mainly by the CAMAC-based data acquisition system at TUDA.

The thick target method [24–28] was used to study the elastic scattering of the beam on protons over a range of incident energies, which range was determined by the energy loss of the beam in the target. Low-density polyethylene ($[\mathrm{CH_2}]_n$) targets with thicknesses of 250 μg/cm^2 were used.

In resonant elastic scattering, ^{22}Mg is formed via sub-Coulomb barrier fusion of $^{21}\mathrm{Na} + p$ as an excited compound nucleus, whose states promptly decay back into $^{21}\mathrm{Na} + p$, with the ^{21}Na in its ground state or in a low-energy excited state. This process interferes with Coulomb elastic scattering leading to the characteristic resonance patterns seen in the excitation function. With the low beam energies used in this experiment, only low-angular-momentum states in ^{22}Mg could be formed via this reaction channel.

Data were obtained at a series of beam energies (580, 690, 800, 880, 990, 1144, 1240, 1340, 1440, and 1560 keV/u) such that the data overlapped in terms of beam energy loss in the target. In this way, a complete excitation function of elastically scattered protons was collected in the center-of-mass range $E = 400$–1500 keV. Typical runs lasted 48 h, thereby enabling sufficient statistics to be collected; the differential cross section for these energies typically ranged from a few hundreds of mb sr^{-1} to around 1 b sr^{-1}. Targets were replaced periodically throughout these runs to avoid problems associated with hydrogen depletion of the polyethylene over time.

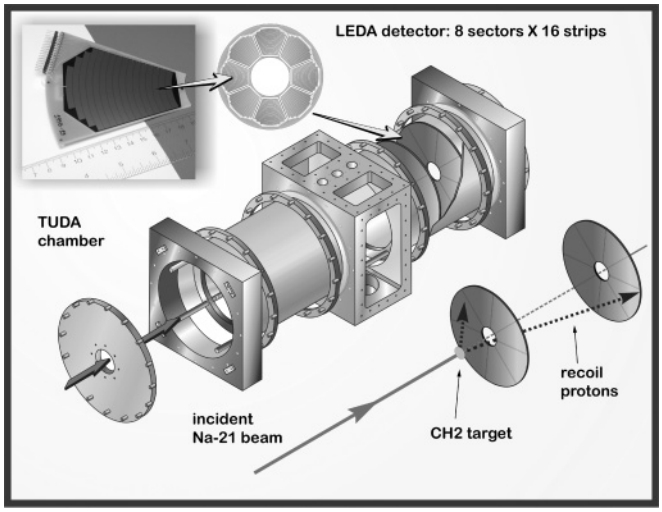

FIG. 1. The TUDA facility with LEDA [29] arrays.

The elastically scattered protons were detected with two LEDA silicon detector arrays [29], covering a laboratory angular range of 4.6°–33° (see Fig. 1 for a schematic of the TUDA experimental setup). In inverse kinematics, this corresponds to looking at angles in the center-of-mass system of 114°–171°. Mylar foils of various thicknesses were used to shield the detectors from scattered beam particles and recoil particles from the carbon content in the target. One sector of the array at larger laboratory angles was left uncovered in order to simultaneously enable the normalization of data via Rutherford scattering of ^{21}Na on carbon. The experimental resolution therefore consisted of small broadening components from the energy loss straggling of the Mylar and within the detector dead layer, combined with the small kinematic broadening from the finite detector strip opening angles and the intrinsic detector resolution.

Data were reduced by sorting events from detector elements at the same angle into annular spectra, and gainmatched via α-particle calibrations. The pulse-height defect associated with the response of protons in silicon compared to α particles was corrected [30]. Reverse energy loss routines, using a parametrization of the Bethe-Bloch formalism [31], were applied to correct for nonlinearities introduced by differential energy loss through the Mylar and detector dead layer.

Nominal beam energies based on calibrations using the DRAGON facility were used to fit the high-energy edges of the proton energy spectra, using comparisons with Monte Carlo simulations developed specifically for this experiment. This methodology, which is described along with the rest of the data reduction procedures in Ref. [32], enables the transformation of the proton energy spectra at each laboratory angle into the interaction center-of-mass energy, since the relationship between these two energies is given by

$$T_p = 4E \frac{m_{\mathrm{Na}}}{m_{\mathrm{Na}} + m_p} \cos^2 \theta_p, \qquad (1)$$

where T_p is the laboratory proton energy, E is the interaction energy in the center-of-mass system, m_{Na} and m_p are the projectile and target masses, and θ_p is the laboratory scattering angle of the proton. Elastic scattering data taken under identical experimental conditions using an 880 keV/u ^{21}Ne beam were used to make fine calibration adjustments to the ^{21}Na + p data via an s-wave resonance in ^{21}Ne + p at $E_{\mathrm{c.m.}} =$ 733 keV corresponding to the $E_x = 7471$ keV 2^+ state in ^{22}Na extensively studied in previous work [33–38].

The experimental resolution in the data from runs with different beam energies and for each angle was determined by comparing Monte Carlo simulations and the shape of the proton spectra. The high-energy edges of the proton spectra were compared to simulation allowing a convolution parameter to be determined, which was modeled as a Gaussian with an energy-dependent width. During the fitting of the experimental data, the calculated excitation function was convoluted with this function before it was compared to the data. Fits of the calibration resonance at 733 keV in ^{21}Ne + p confirmed that the estimated width from the simulation agreed with the convolution required to minimize the χ^2. Typical values of the Gaussian standard deviation in the convolution function were of the order of 5 keV in the center-of-mass system for the inner angles.

Five resonances were observed in the combined elastic and inelastic data, as shown in Figs. 2 and 3. The first resonance at 825 keV was seen in the elastic channel only. The second resonance at 1083 keV shows up as a relatively large peak in the inelastic channel, while appearing as a small distortion in the elastic channel, lying on the low-energy side of the third elastic resonance at 1107 keV. This third resonance is also seen as a small peak in the inelastic channel. The fourth resonance at 1288 keV has a large elastic component and the largest inelastic peak of all the resonances. In the elastic data, the shapes of the first and third resonances were, for the most part, conserved over all the detection angles, while the fourth resonance seemed to rapidly diminish in amplitude at higher angles, suggesting a nonzero partial wave capture. The fifth resonance at 1377 keV was seen only as a small peak in the tail of the 1560-keV/u-thick target spectrum.

IV. MULTICHANNEL *R*-MATRIX ANALYSIS

The ground state spin-parity configurations of ^{21}Na and the proton are $3/2^+$ and $1/2^+$, respectively. This makes the problem of ^{21}Na + p scattering a nonzero spin one, where the channel spin in the elastic channel can have the values $s = 1, 2$. The existence of an excited $5/2^+$ state of ^{21}Na at $E_x = 322$ keV means that above $E_x = 5830$ keV in ^{22}Mg the inelastic scattering channel is open, making ^{21}Na + p scattering a multichannel problem. A spin-zero, single-channel R-matrix formalism was used in the previous publication of this experimental data in order to attempt to derive resonance parameters [7]. This preliminary fit was limited in its success; the use of the inconsistent formalism introduced factors resulting in the underestimation of partial widths and the inaccurate determination of resonance energies. However, the aim of such a fit was to provide estimates of the widths and rough positions of the resonances pending a full analysis. No spin-parity assignments could be made in that analysis.

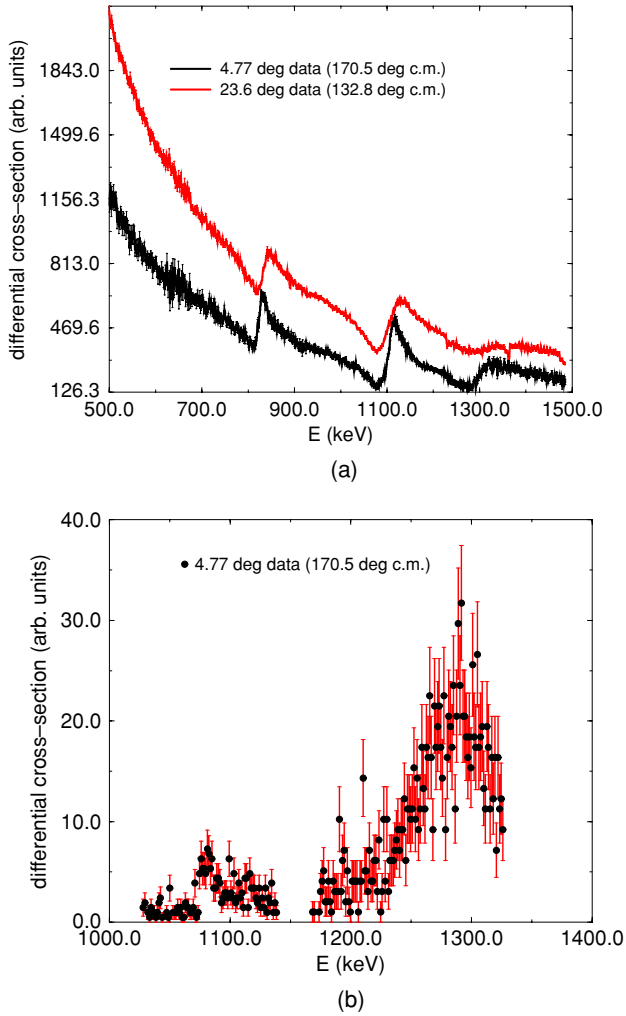

FIG. 2. (Color online) Upper: forward and backward angle data from two detector annuli showing resonances in the elastic channel. Lower: forward angle data showing resonances in the inelastic channel. The y axis shows the differential cross section in arbitrary units.

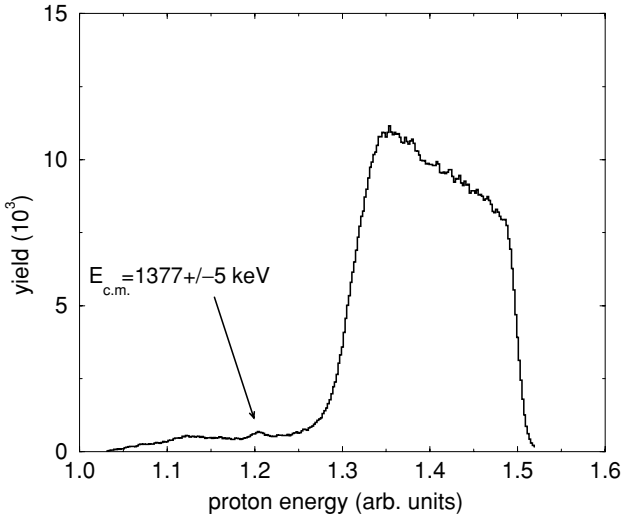

FIG. 3. The 1560 keV/nucleon proton spectrum summed over all inner LEDA angles (4.6°–11.7°), showing the highest energy resonance as an inelastic peak.

A single-channel formalism with the correct summations over different channel spins was used in Ref. [32] in an attempt to fit the elastic data only. Since no inelastic scattering was observed from runs corresponding to the position of the lowest energy elastic resonance ($E_R = 825$ keV), a proton partial width and resonance energy were extracted from the data for this state. The state was assigned a 1^+ configuration and identified as probably being the analog of the 1^+, $E_x = 6854$ keV state in ^{22}Ne. This assignment is consistent with a subsequent shell-model investigation of Fortune *et al.* [39], who also assigned a 1^+ configuration to the state based on Coulomb-shift calculations and previously derived spectroscopic factors.

The multichannel formalism and method used in this work is described in detail in Appendix B.

Initial fits were investigated only for the data from the inner LEDA annulus to determine trends that might assist in a global fit. The low energy resonance was left fixed with values close to those derived in Ref. [32]. The smallest χ^2 for any single angle fit was found to be for the configuration 1^+, 1^-, 2^+, 2^-. The configuration of the fourth resonance was allowed to vary, and the results are shown in Table II. The fits compared to the excitation function can be seen in Fig. 4. With the fourth resonance set at 2^-, fits were attempted on the second resonance in various different configurations. The fits can be seen in Fig. 5, and the resulting R-matrix parameters are listed in Table III.

The best overall fit was that of fit 1, with the configuration $1^+, 1^-, 2^+, 2^-$. The next best fit was that of fit 5, configuration $1^+, 2^-, 2^+, 2^-$. In the former case, the inelastic χ^2_ν was 1.318, in the latter 1.333. In general there is then a preference for the assignment of the configuration 1^- to the second resonance, although the fit for a 2^- configuration is close. Fit 6 had significantly larger (greater than 2.0) values of χ^2_ν over the region of resonance 2, and an inelastic χ^2_ν value of 1.337. An attempt to fit a 3^+ state to this resonance via d-wave capture was unsuccesful in that the resonance would be forced in MINUIT [40] to higher energies resulting in a smaller χ^2_ν than if the resonance were in the correct position; this fit was not included in the results.

For the fits in which the configuration of the fourth resonance was varied, only fit 1 has a value of χ^2_ν less than 2.0 over the region of the resonance. Fits 2 and 3 do not reproduce the shape of the resonance well, while fit 4, although having a χ^2_ν greater than 3 over the resonance region, may be a reasonable fit to the resonance shape. The inelastic χ^2_ν in fit 4 was 3.045, considerably worse than that of fit 1.

Although with the first and third resonances the fits were very discriminating in the sense that no other configuration for each resonance would even closely match the resonance shape, the situation was more ambiguous for the second and fourth resonances. To further constrain the possibilities, it was necessary to consider the physical widths and positions of these resonances result-

TABLE II. Pole energies, reduced partial widths, and fit parameters for fits of the inner LEDA annulus data, for the different possible spin configurations of state 4, all other states being fixed in configuration as shown. The fifth state is the background level described in Appendix B. The labels p and p' denote the elastic and inelastic channel respectively. See Appendix A for an explanation of the parameters.

	Resonance energy (MeV)	State spin J^π	Pole energy E_λ (MeV)	Reaction channel α	Channel spin s	Orbital angular momentum l	Reduced width γ_c (MeV$^{1/2}$)
	0.825	1^+	0.82449	p	1	0	0.68411
Fit 1	1.083	1^-	1.13940	p	1	1	−0.56343
				p	2	1	0.13356
				p'	2	1	0.35748
Elastic $\chi^2_\nu = 1.268$	1.108	2^+	1.13180	p	2	0	0.35273
				p'	2	0	0.08395
Inelastic $\chi^2_\nu = 1.318$	1.290	2^-	1.80220	p	1	1	0.54715
				p	2	1	1.08700
				p'	2	1	−0.88627
				p'	3	1	−0.00019
	Bkgnd. state	1^+	277.940	p	1	0	21.4040
	0.825	1^+	0.82449	p	1	0	0.68411
Fit 2	1.083	1^-	1.19090	p	1	1	0.74682
				p	2	1	0.40169
				p'	2	1	0.32372
Elastic $\chi^2_\nu = 1.620$	1.108	2^+	1.12670	p	2	0	0.31118
				p'	2	0	0.05673
Inelastic $\chi^2_\nu = 1.445$	1.290	1^-	2.67030	p	1	1	0.77494
				p	2	1	−1.66630
				p'	2	1	1.79230
	Bkgnd. state	1^+	277.940	p	1	0	18.6890
	0.825	1^+	0.82499	p	1	0	0.68411
Fit 3	1.083	1^-	1.3257	p	1	1	1.1034
				p	2	1	0.59496
				p'	2	1	0.58008
Elastic $\chi^2_\nu = 2.145$	1.108	2^+	1.1218	p	2	0	0.26654
				p'	2	0	0.04043
Inelastic $\chi^2_\nu = 2.320$	1.290	3^-	1.4330	p	2	1	0.66077
				p'	2	1	−0.48704
				p'	3	1	−0.00034
	Bkgnd. state	1^+	277.940	p	1	0	18.3700
	0.825	1^+	0.82499	p	1	0	0.68411
Fit 4	1.083	1^-	1.4274	p	1	1	−0.10912
				p	2	1	−1.3771
				p'	2	1	0.86548
Elastic $\chi^2_\nu = 2.012$	1.108	2^+	1.1244	p	2	0	0.24054
				p'	2	0	0.04791
Inelastic $\chi^2_\nu = 3.045$	1.290	2^+	1.5357	p	2	0	0.34858
				p'	2	0	0.84119
	Bkgnd. state	1^+	277.940	p	1	0	24.025

ing from the fits and to consider possible analog states in ^{22}Ne.

V. BOUNDARY TRANSFORMATIONS

To calculate resonance energies and experimental widths from the internal *R*-matrix pole parameters, the method of Barker [41] is used. The pole energy of a particular state is equal to the resonance energy for that state when the shift function is equal to the boundary value for each channel. In this work the boundary conditions are calculated at $E = 0.825$ MeV for the elastic channel and $E = 0.503$ MeV for the inelastic channel. For each state the new boundary values $B'(E)$ must be calculated, and the boundary matrix $\mathcal{C}$ of [41] must be calculated via

$$\mathcal{C}_{\lambda\mu} = E_\lambda \delta_{\lambda\mu} - \sum_c (B'_c - B_c)\gamma_{c\lambda}\gamma_{c\mu}. \qquad (2)$$

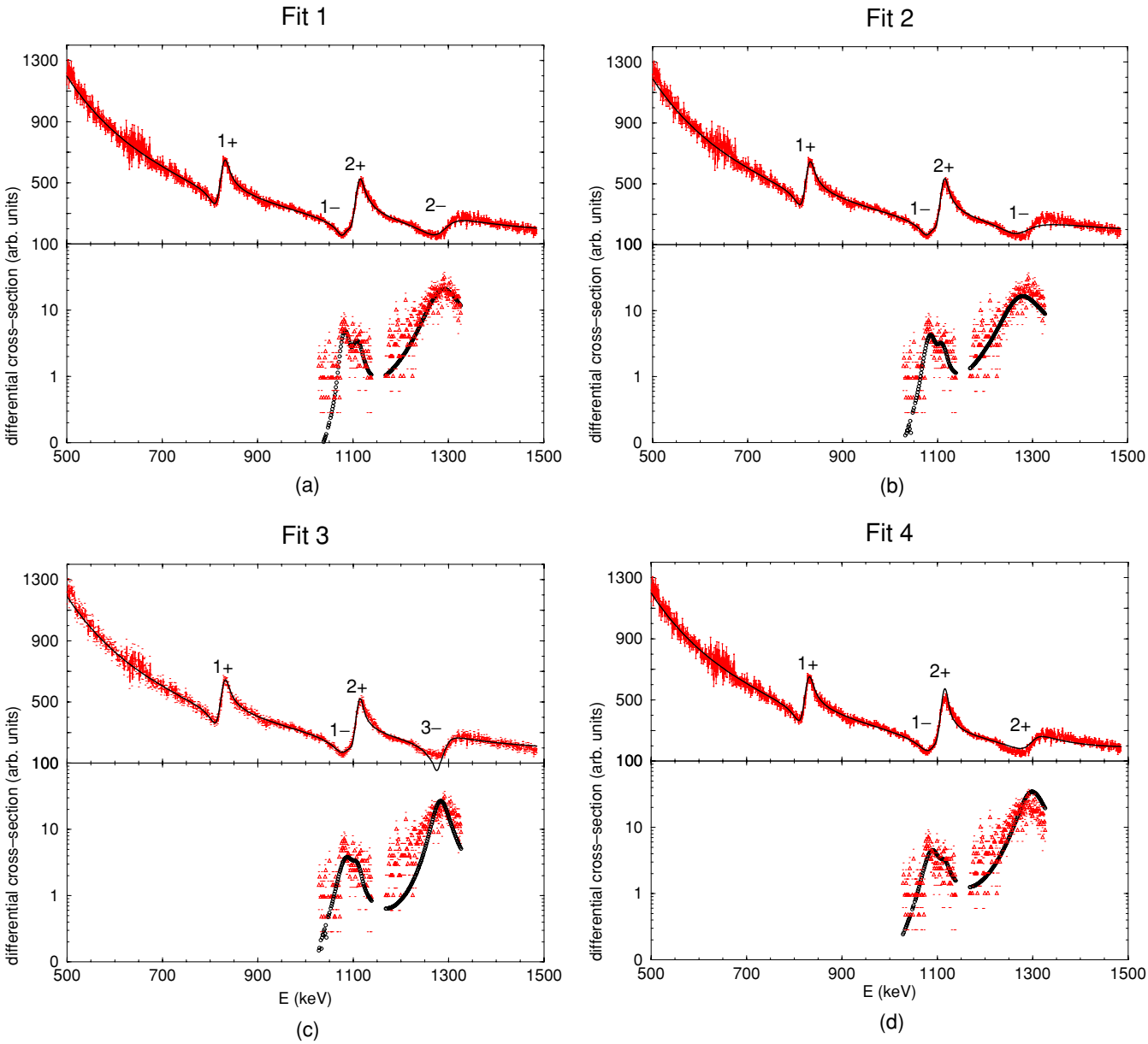

FIG. 4. (Color online) Differential cross-section fits for 4.77° LEDA annulus data, for four spin configurations of state 4.

The subscript c denotes different reaction channels which can occur with differing channel spin and orbital angular momentum; δ is the Kronecker-delta symbol; γ is the reduced width for a particular reaction channel (see Appendixes A and B for a full description of these parameters). The eigenvalues D_λ of this matrix are calculated, as well as the associated eigenvector elements $K_{\lambda\mu}$; the new pole energies and reduced widths are then given by

$$E'_\lambda = D_\lambda \quad \text{and} \quad \gamma'_c = \mathbf{K}\boldsymbol{\gamma}_\mathbf{c}. \tag{3}$$

In this way the boundary energy E is iterated until, for each state, the recalculated pole energy E'_λ from the boundary transformation is equal to E. Then $B(E) = S(E'_\lambda)$ and therefore $E'_\lambda = E_{R,\lambda}$.

The experimentally observed energy-dependent partial widths for the resonances can then be calculated by the relation

$$\Gamma^{\text{exp}}_{c\lambda}(E) = \frac{2\mathcal{P}_c(E)\left(\gamma^R_{c\lambda}\right)^2}{1 + \left(\gamma^R_{c\lambda}\right)^2 \frac{dS(E)}{dE}\big|_{E=E_R}}, \tag{4}$$

where $\gamma^R_{c\lambda}$ is the *on-resonance* reduced partial width for state λ, channel c.

The values of the experimentally observed parameters resulting from the boundary transformation for the ambiguous fits 1, 4, and 5 are listed in Table IV. Dimensionless widths are also listed, using the definition found in the work of Iliadis [42]

$$\theta^2_{\lambda c} = \gamma^2_{\lambda c}\left(\frac{\hbar^2}{m_c r_c^2}\right)^{-1}, \tag{5}$$

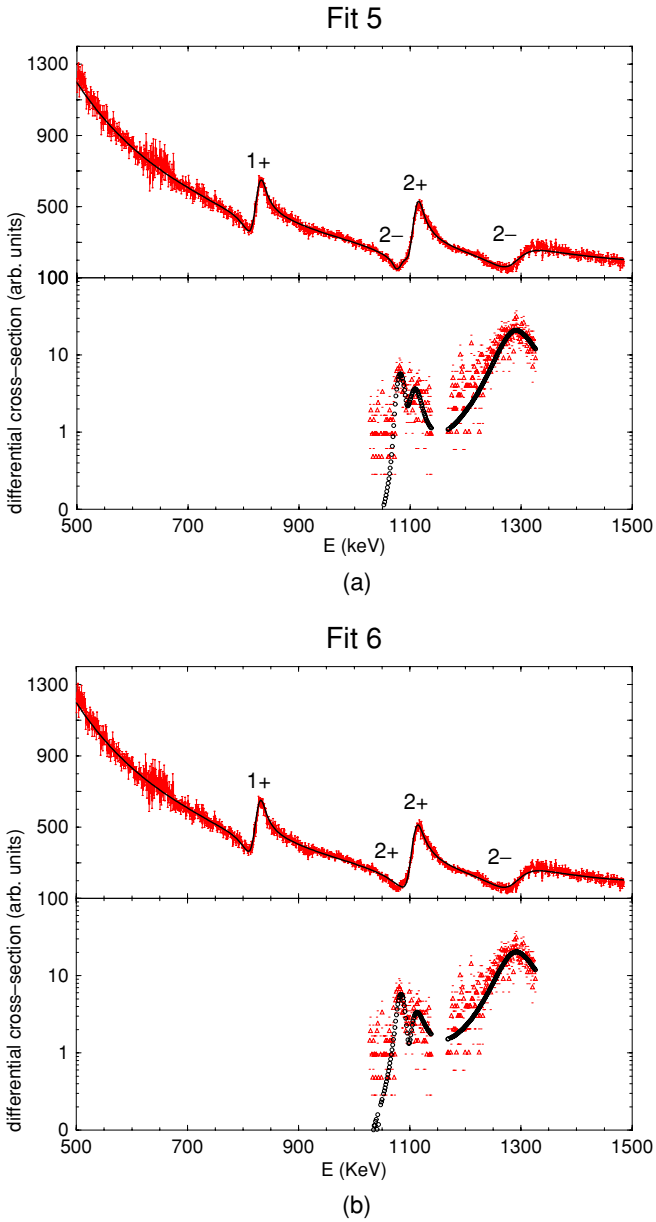

FIG. 5. (Color online) Differential cross-section fits for 4.77° LEDA annulus data, for configurations of $J^\pi = 2^+, 2^-$ for the second resonance.

and the dimensionless width $\theta_{\lambda c}$ is related to the single-particle dimensionless width $\theta_{\rm sp}$ via

$$\theta^2_{\lambda c} = C^2 S \theta^2_{\rm sp}, \tag{6}$$

where C is the isospin Clebsch-Gordan coefficient and S is the spectroscopic factor.

The final fit was made for the data sets at angles 4.77°, 6.58°, 8.38°, and 9.709°. Errors on the resonance energies were calculated from the error in the calibration of the excitation function from detected proton energy into center-of-mass energy. This error is dominated by the uncertainty in the ISAC beam energies. However, the use of the 733 keV resonance in ^{21}Ne + p as a calibration point reduces the error at low energies in the excitation function. Errors in the partial widths were estimated by making fits with the value of the experimental resolution set to its $\pm 1\sigma$ values (as determined via Monte Carlo simulations) and taking the uncertainty in the best-fit parameters as the measure of the error in partial width. The uncertainty introduced by the minimum MINUIT step size used when making the fits was also included in the final error analysis.

VI. DISCUSSION

A. 825 keV resonance; ^{22}Mg (6333 ± 2.4 keV, 1^+)

The energy of this state is closest to the 6322.6 ± 6.0 keV state seen in the (p, t) study of Ref. [14]. The adopted value has since been based solely on that energy. However, the more recent (^{3}He,^{6}He) study of Ref. [17] measured an energy of 6329 ± 6 keV, although based on the same calibration resonance as the (p, t) study. The recent (p, γ) measurement by DRAGON [43] found this resonance to lie at $E_{\rm c.m.} = 821.3 \pm 0.9$ keV, resulting in an excitation energy of 6329 keV, coinciding with the (^{3}He,^{6}He) result. Fortune *et al*. identified this state with the 6854 keV 1^+ state in ^{22}Ne, which is known to have an s-wave spectroscopic factor of 0.57 [39], based on the shell-model and energy-shift calculations. This same conclusion was reached based on similar Thomas-Ehrmann shift calculations in Ref. [32]. The experimental width of 13.6 keV agrees well with the measured width of 16 keV in the (p, γ) measurement of the recent study using the DRAGON recoil separator [43]. Fortune *et al*. also calculated a width of 16 keV for this state based on a single-particle width of 28 keV using the analog state spectroscopic factor.

This state is also likely to be the equivalent of the $T = 1$, 1^+ state at 7408 keV (shown in Fig. 6 at energy 6761 keV because of subtraction of 657 keV, the energy of the first $T = 1$ state in ^{22}Na) in ^{22}Na, that being the only firm 1^+ assignment for a $T = 1$ state within reasonable energy range of 6333 keV that does not already have a known analog in ^{22}Mg.

B. 1083 keV resonance; ^{22}Mg [6591 ± 10 keV, (1^-)]

This previously unobserved state is well described by a p-wave resonance in the elastic channel. The best fit occurs for $J^\pi = 1^-$, although the fit for $J^\pi = 2^-$ is not significantly worse. For both configurations (fits 1 and 4), a similar resonance energy is obtained. In the 1^- case, a partial elastic width via the $s = 1$ channel spin is preferred over the $s = 2$ partial width; while in the 2^- case, similar partial elastic widths are obtained for $s = 1, 2$. The resulting total widths of 13 and 6 keV are consistent with the apparent width of this resonance estimated in Ref. [32]. The fact that there are no known 2^- states in ^{22}Ne or ^{22}Na in this energy range suggests that the state is more likely the 1^- configuration. There are two possible analog 1^- states in ^{22}Ne. The first, at 6691 keV, is populated only weakly in the ^{21}Ne$(d, p)^{22}$Ne reaction of Ref. [44], but populated more strongly in the ^{18}O(^{7}Li, $t)^{22}$Ne study of Ref. [45]. No (d, p) spectroscopic factor is therefore known for this state. The second state at 7052 keV has a known (d, p) spectroscopic factor of 0.018; however, this state probably has an analog in ^{22}Mg at a much higher energy than 6591 keV, possibly well

TABLE III. Pole energies, reduced partial widths, and fit parameters for fits of the inner LEDA annulus data, for some different possible spin configurations of state 2, all other states being fixed in configuration as shown (the 1^- configuration is fit 1 of Table II). The fifth state is the background level described in Appendix B. The labels p and p' denote the elastic and inelastic channel respectively. See Appendix A for an explanation of the parameters.

	Resonance energy (MeV)	State spin J^π	Pole energy E_λ (MeV)	Reaction channel α	Channel spin s	Orbital angular momentum l	Reduced width γ_c (MeV$^{1/2}$)
	0.825	1^+	0.82449	p	1	0	0.68411
Fit 5	1.083	2^-	1.1045	p	1	1	−0.28173
				p	2	1	0.24246
				p'	2	1	0.21056
Elastic $\chi^2_\nu = 1.290$	1.108	2^+	1.13290	p	2	0	0.35984
				p'	2	0	0.08662
Inelastic $\chi^2_\nu = 1.333$	1.290	2^-	1.80580	p	1	1	0.48737
				p	2	1	1.11290
				p'	2	1	−0.89195
				p'	3	1	0.00048
	Bkgnd. state	1^+	277.940	p	1	0	21.7830
	0.825	1^+	0.82449	p	1	0	0.68411
Fit 6	1.083	2^+	1.1274	p	2	0	−0.30393
				p'	2	0	0.26373
Elastic $\chi^2_\nu = 1.392$	1.108	2^+	1.1647	p	2	0	0.27581
				p'	2	0	0.63240
Inelastic $\chi^2_\nu = 1.338$	1.290	2^-	1.80090	p	1	1	0.40551
				p	2	1	1.16300
				p'	2	1	−0.84279
				p'	3	1	0.00012
	Bkgnd. state	1^+	277.940	p	1	0	22.7220

above 6800 keV. It is therefore suggested that the 6591 keV state is a 1^- configuration and is the analog of the 6691 keV state in ^{22}Ne. These states probably carry through into the ^{22}Na $T = 1$ system via the tentative $(1^-, 2^+)$ state at 7277 keV, if this state turns out to be a 1^- configuration. There are no other known 1^-, $T = 1$ states in ^{22}Na within a reasonable energy range.

C. 1107 keV resonance; ^{22}Mg (6615 ± 11 keV, 2^+)

The measured excitation energy is equal to the 6616 ± 4 keV measured in the (^{3}He,^{6}He) study of Ref. [17], compared to the energy of 6608.5 ± 5.6 keV measured in the (p, t) study of Ref. [14]. This state is almost certainly the analog of the 6819 keV, 2^+ state in ^{22}Ne, which is known to have an s-wave spectroscopic factor of 0.18 [39]. Indeed Fortune *et al*. also suggested this assignment based on their Coulomb energy calculations and, using a calculated value of 105 keV for the single-particle width of this state (assuming s wave), arrive at an estimated resonance width of 19 keV, which is in excellent agreement with the measured value of 18 keV in this work.

This state is also probably the analog of the known 2^+, $T = 1$ state at 7471 keV in ^{22}Na.

D. 1288 keV resonance; ^{22}Mg [6796 ± 17 keV, (1^-,2^-)]

The excitation energy of this state is close to that of the state at 6787 keV measured by Bateman *et al*. [14] in the (p, t) study. However, other experiments have measured varying values of excitation energy for this state, ranging from 6760 to 6836 keV. A previous assignment of 3^- to this state was included in the literature based on the distorted-wave Born approximation (DWBA) fits to the (^{3}He, n) data of Ref. [11]; however, the data of that work show that the peak corresponding to the 6798 keV state is not completely resolved from the peak corresponding to the 6884 keV state. The DWBA fits for both these states seem to exhibit similar properties, leading to the possibility that there exists a component of each angular distribution in the other. It is therefore suggested that such a spin-parity assignment be taken as tentative rather than firm. Indeed our data seem to suggest that the preferred configuration of this state is 1^- or 2^-.

E. 1377 keV resonance; ^{22}Mg (6885 keV)

The excitation energy of this state is closest to that of the 6884 keV state. No spin-parity assignment exists for this state and in this work no assignment was made. This state was seen only as a weak peak in the inelastic channel and was subsequently not included in the R-matrix analysis.

The results of this work and of these assignments are shown in Table V; the analog system level scheme, indicating the assignments made, is shown in Fig. 6.

VII. CONCLUSIONS

The spin-parity assignments made in this work help clarify the structure of the $A = 22$, $T = 1$ system below

TABLE IV. Experimental widths and resonance energies for the three best fits 1, 4, and 5, as determined by the boundary transformation method.

Fit	Resonance (J^π)	Energy (keV)	Widths (keV)	l value	Spin	$\theta^2_{\lambda c}$
1	1 (1^+)	824.8	$\Gamma_p = 13.6$	s-wave	1	0.55
			$\Gamma_{\text{tot}} = 13.6$			
	2 (1^-)	1082.9	$\Gamma_p = 11.3$	p-wave	1	0.45
			$\Gamma_p = 0.8$	p-wave	2	0.11
			$\Gamma_{p'} = 0.7$	p-wave	2	0.28
			$\Gamma_{\text{tot}} = 12.8$			
	3 (2^+)	1107.6	$\Gamma_p = 17.0$	s-wave	2	0.28
			$\Gamma_{p'} = 0.19$	s-wave	2	0.06
			$\Gamma_{\text{tot}} = 17.19$			
	4 (2^-)	1290.1	$\Gamma_p = 23.1$	p-wave	1	0.44
			$\Gamma_p = 65.5$	p-wave	2	0.87
			$\Gamma_{p'} = 12.7$	p-wave	2	0.69
			$\Gamma_{p'} = 0.0$	p-wave	3	0.00
			$\Gamma_{\text{tot}} = 101.3$			
4	1 (1^+)	824.8	$\Gamma_p = 13.6$	s-wave	1	0.55
			$\Gamma_{\text{tot}} = 13.6$			
	2 (2^-)	1081.9	$\Gamma_p = 3.1$	p-wave	1	0.22
			$\Gamma_p = 2.5$	p-wave	2	0.20
			$\Gamma_{p'} = 0.25$	p-wave	2	0.16
			$\Gamma_{p'} = 0.0$	p-wave	3	0.00
			$\Gamma_{\text{tot}} = 5.9$			
	3 (2^+)	1107.6	$\Gamma_p = 17.7$	s-wave	2	0.29
			$\Gamma_{p'} = 0.2$	s-wave	2	0.07
			$\Gamma_{\text{tot}} = 17.9$			
	4 (2^-)	1289.1	$\Gamma_p = 20.0$	p-wave	1	0.40
			$\Gamma_p = 67.5$	p-wave	2	0.89
			$\Gamma_{p'} = 13.7$	p-wave	2	0.72
			$\Gamma_{p'} = 0.0$	p-wave	3	0.00
			$\Gamma_{\text{tot}} = 101.2$			
5	1 (1^+)	824.8	$\Gamma_p = 13.6$	s-wave	1	0.55
			$\Gamma_{\text{tot}} = 13.6$			
	2 (1^-)	1090.5	$\Gamma_p = 0.5$	p-wave	1	0.09
			$\Gamma_p = 40.9$	p-wave	2	1.11
			$\Gamma_{p'} = 3.7$	p-wave	2	0.70
			$\Gamma_{\text{tot}} = 45.1$			
	3 (2^+)	1111.3	$\Gamma_p = 10.3$	s-wave	2	0.22
			$\Gamma_{p'} = 0.4$	s-wave	2	0.09
			$\Gamma_{\text{tot}} = 10.7$			
	4 (2^+)	1299.9	$\Gamma_p = 22.7$	s-wave	2	0.24
			$\Gamma_{p'} = 40.1$	s-wave	2	0.66
			$\Gamma_{\text{tot}} = 62.8$			

6900 keV. The 1^+ resonance at 6333 keV and the 2^+ resonance at 6616 keV are paired with the states in ^{22}Ne at 6854 and 6819 keV, respectively. This means that there are no other known low-spin positive parity states in ^{22}Ne below 6900 keV *without* assigned mirror states in ^{22}Mg, with the exception of the $(2, 3)^+$ state at 6636, which is known to have zero s-wave strength anyway [44]. Therefore it is probable that no previously unobserved s-wave resonances important to the ^{21}Na$(p, \gamma)^{22}$Mg reaction rate exist below 6900 keV. This argument is confirmed by the consideration of known $T = 1$ states in ^{22}Na: Nearly every state above the ^{21}Na $+ p$ threshold up to 6798 keV can be accounted for in ^{22}Na (see Fig. 6). This is important given that several experimental programs currently exist which aim to use a variety of different methods to find additional contributing resonances in ^{21}Na $+ p$. Of course, this argument fails if there are undiscovered low-spin positive parity states in ^{22}Ne. However, the shell model predicts very well the known ordering of these states in ^{22}Ne, as demonstrated in the work of Fortune *et al*. [39], and all known positive parity states below 6900 keV are accounted for in

TABLE V. Experimental resonance energies, widths, and spin-parity assignments for ^{21}Na + p data, including suggested analog assignments in ^{22}Ne.

Resonance energy (keV)	J^π	Experimental widths (keV)	l	Excitation energy in ^{22}Mg (keV)	Analog state in ^{22}Ne (keV)
824.8 ± 2.4	1^+	$\Gamma_{\text{tot}} = 13.6 \pm 1.4$		6332.8 ± 2.4	6853.5 ± 0.12
		$\Gamma_p = 13.6 \pm 1.4$	0		
1082.5 ± 10.0	(1^-)	$\Gamma_{\text{tot}} = 12.8 \pm 1.51$		6590.5 ± 10.0	6691 ± 4
		$\Gamma_p = 11.9 \pm 1.4$	1		
		$\Gamma_{p'} = 0.94 \pm 0.11$	1		
1107.2 ± 10.8	2^+	$\Gamma_{\text{tot}} = 17.9 \pm 1.6$		6615.2 ± 10.8	6819.4 ± 0.16
		$\Gamma_p = 17.6 \pm 1.5$	0		
		$\Gamma_{p'} = 0.3 \pm 0.1$	0		
1287.5 ± 17.0	$(1^-, 2^-)$	$\Gamma_{\text{tot}} = 105.0 \pm 32.8$		6795.5 ± 17.0	
		$\Gamma_p = 93.9 \pm 32.0$	1		
		$\Gamma_{p'} = 11.1 \pm 0.8$	1		

this case; in fact the only states not included in the shell-model estimate are the 1^- state at 6691 keV (paired with our measured 1^- state at 6591 keV in ^{22}Mg) and the 3^- state at 5910 keV.

It is known from the DRAGON studies [43] that resonant capture to the 6333 keV 1^+ state and the 6248 keV state (corresponding to a resonance energy of 738 keV) in ^{22}Mg will dominate the reaction rate above temperatures of 1.1 GK, too high for novae, but perhaps interesting in the consideration of nucleosynthesis within the accretion disks of x-ray binaries. Higher energy resonances than this are simply not broad or strong enough to affect the reaction rate at low temperatures. However, one must also consider the radiative capture from the first excited state of ^{21}Na at 332 keV, which will be populated in a thermal bath at astrophysical temperatures. The ratio of the population of the first excited state to the population of the ground state in full thermal equilibrium is given

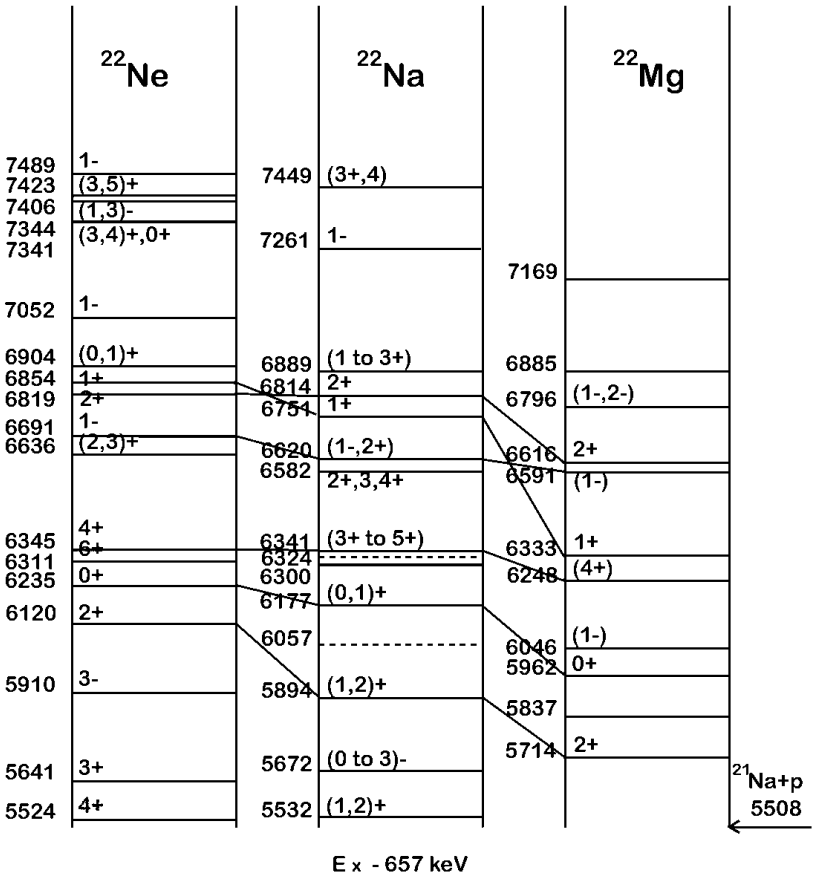

FIG. 6. The $A = 22$, $T = 1$ analog system showing suggested mirror states for the three levels assigned with spin-parity values in this work. The level energies in the ^{22}Na scheme are the excitation energies of the $T = 1$ states minus 657 keV, the energy of the lowest $T = 1$ state, in order to bring them in line with the $T = 1$ structure of ^{22}Ne and ^{22}Mg.

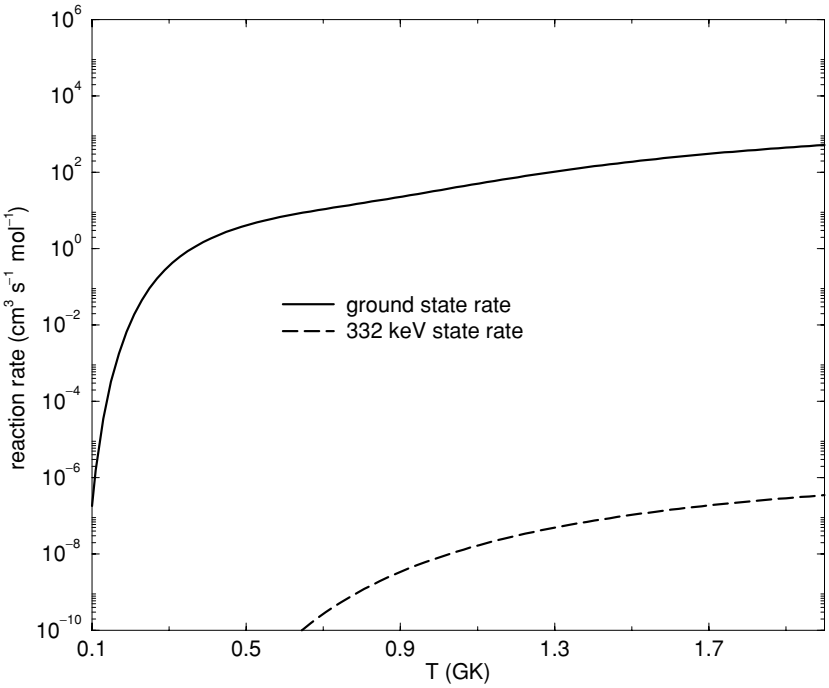

FIG. 7. Total ^{21}Na(p, γ)^{22}Mg reaction rate as calculated using resonance strengths from ref. [43] and the partial widths measured in this work. Capture from the thermally populated first excited state of ^{21}Na ($E_x = 332$ keV) is included.

by

$$\frac{n_1}{n_0} = \frac{g_1}{g_0} \exp(-E_x/kT), \tag{7}$$

where $g_i = 2J_i + 1$. Thus the total reaction rate (ground state and first excited state) can be written as

$$\langle \sigma v \rangle_{\text{tot}} = N_A \left(\langle \sigma v \rangle_0 + \frac{n_1}{n_0} \langle \sigma v \rangle_1 \right). \tag{8}$$

We calculated both reaction rates per particle pair using the resonance parameters supplied in the DRAGON study [43] and the results of this work. The resonances seen in this work were treated as broad, and therefore the rate was calculated by numerical integration. All lower energy resonances were treated using the narrow resonance formalism. The γ widths of the 825 and 1108 keV resonances were calculated from the DRAGON (p, γ) resonance strength measurements and the proton partial widths determined in this work, via

$$\Gamma_\gamma = \frac{\Gamma_p + \Gamma_{p'}}{\omega \Gamma_p / \omega\gamma - 1}. \tag{9}$$

The Γ width for the 1083 keV resonance was estimated via the lifetime of the analog state at 6691 keV in ^{22}Ne. The Γ width of the 1290 keV resonance was set to 1 eV, since its analog state is not known.

The energy dependence of the partial proton widths was treated using a parametrization in terms of the proton width on-resonance and the penetrability, that is,

$$\Gamma_p(E) = \Gamma_p(E_R) \sqrt{\frac{E}{E_R}} \frac{P_l(E, r)}{P_l(E_R, r)}. \tag{10}$$

Figure 7 shows the resulting reaction rate. The dashed curve is the unthermalized reaction rate from the first excited state (the rate assuming equal population of the ground state and first excited state, with no thermal excitation or decay between those states). The black solid curves, which are indistinguishable, are the ground-state reaction rate, and the total reaction rate, taking into account the thermal population of the first excited state and its subsequent capture. The rate from the first excited state is so small that it makes negligible difference to the total rate. The conclusion of this work therefore is that the rates found in this calculation are not significantly different from those found in the DRAGON work [43], with the 206 keV resonance dominating at nova temperatures and the 825 keV resonance becoming dominant above $T = 1.1$ GK.

ACKNOWLEDGMENTS

The authors would like to acknowledge the help of Richard Azuma, Eric Vogt, and Peter Jackson for useful discussions on the development of the *R*-matrix code and preparation of this manuscript. The authors acknowledge the financial support of the Engineering and Physical Sciences Research Council (EPSRC) in the UK for this experimental work, and for the funding of the Ph.D. project associated with it [32]. Financial support from the Natural Sciences and Engineering Research Council of Canada (NSERC) is also gratefully acknowledged. The technical support of TRIUMF and ISAC staff is acknowledged, particularly that of R. Laxdal and M. Pasini for the beam tuning, and M. Dombsky for the radioactive beam production.

APPENDIX A: *R*-MATRIX PARAMETERS GLOSSARY

Table VI lists the notation and symbols of the multichannel *R*-matrix formalism of Lane and Thomas [46].

TABLE VI. Glossary of terms used in *R*-matrix formalism of Ref. [46]. Primed quantities denote values in the exit channel.

I_1	Projectile spin
I_2	Target spin
E	Relative energy in center of mass
Indices:	
α	Channel index
s	Channel spin index
l	Orbital angular momentum index
J	Compound state spin index
λ, μ	Level indices
L	Angular momentum summation index $0 \leqslant L \leqslant \lvert J_1\rvert + \lvert J_2\rvert$
Quantities independent of bound-state properties:	
$\mathrm{k}_\alpha(\mathrm{E})$	Wave number for channel α
$\theta_{\alpha'}$	Exit channel scattering angle in c.m. frame
$\mathrm{C}_{\alpha'}(\mathrm{E})$	Coulomb scattering amplitude for exit channel
$\mathrm{P}_l(\cos\theta_{\alpha'})$	Legendre polynomial
$\mathcal{P}_{\alpha l}(\mathrm{E})$	Penetrability
$S_{\alpha l}(\mathrm{E})$	Energy shift-function
$B_{\alpha l}$	Boundary parameter
r_α	Channel radius
$\bar{Z}$	Racah-like angular momentum factors
$\omega_{\alpha l}(\mathrm{E})$	Coulomb phase shift
$\phi_{\alpha l}(\mathrm{E})$	Hard-sphere phase shift
$F_{\alpha l}(\mathrm{E})$, $G_{\alpha l}(\mathrm{E})$	Regular and irregular solutions to Coulomb wave function
Quantities dependent on bound-state properties:	
$\gamma^J_{\lambda\alpha sl}$	Reduced partial width for level λ
E^J_λ	Pole energy for level λ
$A_{\lambda\mu}$	Level matrix element
$U^J_{\alpha' s' l', \alpha s l}$	Collision matrix element
$T^J_{\alpha' s' l', \alpha s l}$	Transition matrix element

APPENDIX B: MULTICHANNEL *R*-MATRIX FORMALISM

The multichannel formalism used here follows the standard *R*-matrix theory of Lane and Thomas [46]. The differential cross section for a scattering process via entrance channel α to an exit channel α' for given entrance and exit spin channels s and s' is given by a corrected version of Eq. VIII(2.6) of [46] by L. Buchmann (Lane and Thomas omitted the Kronecker delta in the third component of the sum, and by not conjugating the T in the same term, they had a definite error):

$$\begin{aligned}(2s+1)\frac{k_\alpha^2}{\pi} d\sigma_{\alpha s,\alpha' s'} d\Omega_{\alpha'} &= (2s+1)|C_{\alpha'}(\theta_{\alpha'})|^2 \delta_{\alpha' s',\alpha s} \\ &+ \frac{1}{\pi}\sum_L B_L(\alpha' s', \alpha s) P_L(\cos\theta_{\alpha'}) - \delta_{\alpha' s',\alpha s}(4\pi)^{-\frac{1}{2}} \\ &\times \sum_{Jl}(2J+1) 2\Re\left[i\left(T^J_{\alpha' s' l',\alpha s l}\right)^* C_{\alpha'}(\theta_{\alpha'}) P_l(\cos\theta_{\alpha'})\right].\end{aligned} \tag{B1}$$

This can be identified as the sum of separate Coulomb, resonant, and interference terms. In the resonant term, the coefficients B_L are given by

$$\begin{aligned}B_L(\alpha' s', \alpha s) = \frac{1}{4}(-1)^{s-s'} \sum_{J_1 J_2 l_1 l_2 l_1' l_2'} &\bar{Z}(l_1 J_1 l_2 J_2, sL) \\ &\times \bar{Z}(l_1' J_1 l_2' J_2, s' L)\left(T^{J_1}_{\alpha' s' l_1', \alpha s l_1}\right)\left(T^{J_2}_{\alpha' s' l_2', \alpha s l_2}\right)^*.\end{aligned} \tag{B2}$$

The only terms in these equations that involve the description of internal bound states are the transition matrices **T**. This is important because it essentially defines how the fitting program constructs the cross-section values prior to its chi-squared reduction procedure. The more terms that can be left out of the minimizing subroutine, the faster the fitting process becomes.

The method chosen to construct the transition matrices is the *level matrix* approach [47]. The transition matrices are constructed from the *collision matrix*

$$T^J_{\alpha' s' l', \alpha s l} = e^{2i\omega_{\alpha l}} \delta_{\alpha' s' l', \alpha s l} - U^J_{\alpha' s' l', \alpha s l}, \tag{B3}$$

which results from a sum over the level matrix **A**

$$\begin{aligned}U^J_{\alpha' s' l', \alpha s l} = e^{i[(\omega_{\alpha l}+\omega_{\alpha' l'})-(\phi_{\alpha l}+\phi_{\alpha' l'})]}\delta_{\alpha' s', \alpha s} \\ + 2i\sqrt{\mathcal{P}_{\alpha l}} \sum_{\lambda\mu} \gamma^J_{\lambda\alpha s l} \gamma^J_{\mu\alpha' s' l'} A_{\lambda\mu} \sqrt{\mathcal{P}_{\alpha' l'}},\end{aligned} \tag{B4}$$

defined by its inverse

$$(A^{-1})_{\lambda\mu} = \left(E^J_\lambda - E\right)\delta_{\lambda\mu} - \sum_{\alpha sl} \gamma^J_{\lambda\alpha sl}\gamma^J_{\mu\alpha' s' l'}(S_{\alpha l} - B_{\alpha l} + i\mathcal{P}_{\alpha l}). \quad \text{(B5)}$$

The reduced partial widths and pole energies $\gamma^J_{\lambda\alpha sl}$, E_λ are the free parameters in the fit. All other parameters, such as the boundary conditions $B_{\alpha l}$, the energy shift functions $S_{\alpha l}$, and the penetrabilities $\mathcal{P}_{\alpha l}$ are calculated at program initialization time, while the level matrix, collision matrix, transition matrix, and cross section are calculated from these and the freely varying reduced widths within the minimizing routine. Other parameters calculated at initialization are the Coulomb and hard-sphere phase shifts $\omega_{\alpha l}$ and $\phi_{\alpha l}$, and the Racah-like angular momentum addition terms $\bar{Z}$.

The observed differential cross sections, to be compared to the experimental data, are given by summing over channel spins, that is,

$$d\sigma_{\alpha\alpha'} = \frac{1}{(2I_1+1)(2I_2+1)}\sum_{ss'}(2s+1)d\sigma_{\alpha s,\alpha' s'}. \quad \text{(B6)}$$

A. Fitting procedure

The number of free parameters varied depending on the chosen spin-parity configurations of the levels. Here we describe the parameters required for each observed resonance in turn.

825 keV resonance

The lowest energy resonance was found previously in [32] to require a 1^+ configuration, via *s*-wave capture. This requires one pole energy E^1_1 and one reduced partial width γ^1_{1110} since $l = 0$ can only couple to a 1^+ state via channel spin $s = 1$ in this case. Although the $l = 2$ channel is also open in this case, the amplitudes for this will be small based on penetrability arguments. It was found that including $l = 2$ widths in the fit had negligible consequences.

1083 keV resonance

The second lowest resonance has almost no discernible strength in the elastic channel and yet it has a significant inelastic component. This makes the possibility of *s*-wave capture in the entrance channel least probable since the elastic component, even for a small partial elastic width, would show more strongly as a typical *s*-wave shape, given the implied total width from the inelastic peak. Although *p*-wave capture would seem to better explain the observed distortion in the elastic spectrum at the position of this resonance, *d* wave capture is also a possibility since in such a case there may be an *s* wave component to the exit channel leading to the comparatively large inelastic strength observed.

Fits were employed setting this resonance to 2^+ for *s*-wave capture, requiring the free parameters

$$J^\pi = 2^+ :\ E^2_2,\ \gamma^2_{2120},\ \gamma^2_{2220}.$$

This was chosen because of the existence of 2^+ states in ^{22}Ne at energies close to that of this resonance without known analog states in this region of ^{22}Mg.

Fits for *p*-wave capture were also investigated setting this resonance to 1^- and 2^- configurations, requiring

$$J^\pi = 1^- :\ E^1_2,\ \gamma^1_{2111},\ \gamma^1_{2121},\ \gamma^1_{2221},$$

$$J^\pi = 2^- :\ E^2_2,\ \gamma^2_{2111},\ \gamma^2_{2121},\ \gamma^2_{2221}.$$

The existence of a possible 3^+ state at 6636 keV in ^{22}Ne with a known *s*-wave spectroscopic factor of zero, and a *d*-wave spectroscopic factor of 0.1 [39] prompted a fit of this resonance as a 3^+ configuration, *d*-wave in the entrance channel and *s*-, *d* waves in the exit channel, requiring

$$J^\pi = 3^+ :\ E^3_2,\ \gamma^3_{2112},\ \gamma^3_{2122},\ \gamma^3_{2230},\ \gamma^3_{2222},\ \gamma^3_{2232}.$$

1107 keV resonance

We attempted to fit the third resonance with both 1^+ and 2^+ configurations via $l = 0$ in the entrance (elastic) channel, based on the observation that the morphology of the resonance shape closely resembles a typical *s*-wave shape over the angular range of the data, much like the lowest resonance. The inelastic peak is small for this resonance, and the single-channel fit strongly favors a 2^+ configuration. The pole energy E^2_3 is a required free parameter, as well as the elastic reduced partial width γ^2_{3120}. However, this state can couple to the inelastic exit channel via channel spin $s' = 2, 3$. For $s' = 2$, this may occur coupled with $l' = 0$ or $l' = 2$, requiring two reduced partial widths. For $s' = 3$ this can couple via $l' = 2$ only. It was found that the first-order partial wave $l' = 0$ was the only requirement in fitting, since the addition of the $l' = 2$ component did not significantly enhance the cross section. Therefore, for this level the inelastic reduced partial width γ^2_{3220} was a free parameter, making the number of free parameters for this level equal to 3.

1288 keV resonance

The fourth resonance least resembles an *s* wave out of the three large elastic resonances seen in the data. The amplitude of this resonance falls off more rapidly at larger angles, consistent with either the Legendre polynomial contribution from higher *l* values, or substantial broadening of an already low amplitude resonance. Due to the large visible width of this resonance, it is unlikely that it is formed via $l = 2$ or higher from penetrability arguments, leading to the conclusion that this is either a negative parity state formed via $l = 1$, or a broadened *s*-wave capture. States of $J^\pi = (0\text{–}3)^-$ may be formed via $l = 1$ coupled with $s = 1, 2$. However, the existence of a large inelastic component in the data eliminates the possibility of a 0^- configuration which cannot couple with $s' = 2, 3$ via a significantly low odd value of exit orbital angular momentum, i.e., $l' = 1$. The parameters required for the *p*-wave fits were

$$J^\pi = 1^- :\ E^1_4,\ \gamma^1_{4111},\ \gamma^1_{4121},\ \gamma^1_{4221},$$

$$J^\pi = 2^- :\ E^2_4,\ \gamma^2_{4111},\ \gamma^2_{4121},\ \gamma^2_{4221},\ \gamma^2_{4231},$$

$$J^\pi = 3^- : \; E_4^3, \; \gamma_{4121}^3, \; \gamma_{4221}^3, \; \gamma_{4231}^3.$$

A fit for s-wave capture to 2^+ was also investigated, based on the existence of possible 2^+ analog states in ^{22}Ne,

$$J^\pi = 2^+ : \; E_4^2, \; \gamma_{4120}^2, \; \gamma_{4220}^2.$$

The fifth resonance at 1377 keV was not included in the present R-matrix fits, although its position was determined from the energy of the inelastic peak.

A background level was used in the fit to simulate the contributions from higher lying states. Although a rigorous fit should use a background level for each spin configuration represented in the fit, it was found that simply including one background term of 1^+ configuration was sufficient to fit the data. The parameters E_5^1 and γ_{5120}^1 were used for this.

In addition to the resonance parameters, a normalization factor was included as a fit parameter. The best fit value of this from the global four-angle fit was 1.8939 ± 0.0014.

B. Inclusion of optical-model phase shifts

During fitting it was found that the R-matrix analysis overestimated the cross section for center-of-mass energies greater than about 1 MeV. The contribution causing this was found to be from the *hard-sphere phase shift*, which represents potential (elastic) scattering from the nuclear surface. The usual hard-sphere scattering phase shift implemented in the R matrix is given by

$$\phi_{\alpha l} = \arctan \frac{F_{\alpha l}}{G_{\alpha l}} \tag{B7}$$

and represents scattering from a square well. It is possible to replace the square potential with a more realistic Woods-Saxon potential and to simply substitute the hard-sphere phase shift with a phase shift derived from this [48]. This can be done using optical-model calculations for the $^{21}\mathrm{Na} + p$ system. Phase shift substitutions have been performed successfully in previous R-matrix fitting of resonance data (see for example, Namoshi *et al.* [49]).

The optical-model calculations were made with a modified version of the search code HIOPTIM version 03.4 [50]. This code calculates the scattering matrix elements $S_l(l, J)$ and their real and imaginary parts $S_R(l, J)$ and $S_I(l, J)$; the code was altered to output the transmission coefficients $T(l)$ via

$$T(l) = 1 - S_l^2(l, J), \tag{B8}$$

and the nuclear phase shifts $\phi(l)$ via

$$\phi(l) = \frac{1}{2} \tan^{-1}[S_R(l, J), S_I(l, J)]. \tag{B9}$$

A similar modification was inserted where the Coulomb phase shifts $\omega(l)$ were calculated from a high-l series approximation and iterated down to $l = 0$.

In general, the shape of the calculated differential cross sections at very low energies is not very sensitive to the optical-model parameters, but the main difficulty for calculations at astrophysical energies is twofold. First, there are few published parameters for the (projectile) nucleus + proton system, since the projectile is often a radioactive species and obviously has never been studied in normal kinematics, and there are still too few optical-model studies in inverse kinematics with radioactive beams. Second, even when there are published parameters for the chosen nucleus, the optical parameters are usually published for beam energies that far exceed those used in most astrophysics experiments. Thus the best strategy is to choose a global prescription of the optical parameters whose values have a dependence upon Z, N, and A and also upon the beam energy E.

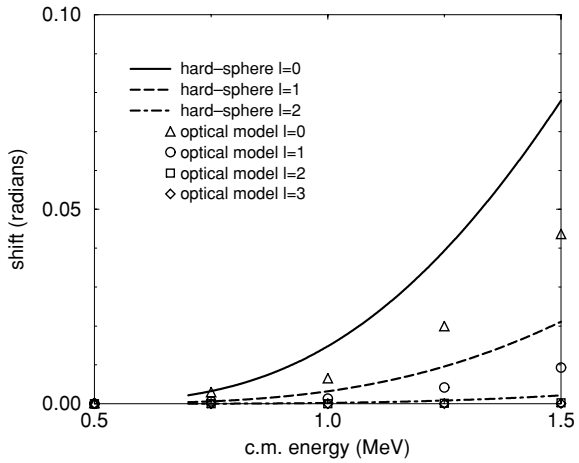

FIG. 8. Comparison between calculated hard-sphere and optical-model phase shifts for partial waves from $l = 0$–3, in the $^{21}\mathrm{Na} + p$ system between 0.5 and 1.5 MeV.

For this work, we chose the prescription of Becchetti and Greenlees [51]; their parameters were obtained by global fits to many datasets at many energies. The real potential has a standard Woods-Saxon shape

$$V(r) = \frac{-V_R}{1 + \exp(X_R)}, \tag{B10}$$

with $X_R = (r - R_R)/a_R$, where V_R is the potential depth, R_R is the radius parameter, and a_R is the diffuseness. A two-component imaginary potential comprises a Woods-Saxon shape plus a first-derivative Woods-Saxon shape with the same geometric parameters

$$W(r) = \frac{-W_I}{1 + \exp(X_I)} - 4W_{\mathrm{der}} \frac{\exp(X_I)}{[1 + \exp(X_I)]^2}, \tag{B11}$$

with $X_I = (r - R_I)/a_I$. A spin-orbit potential is also included of the form

$$V_s(r) = V_{\mathrm{so}} \left(\frac{\hbar}{m_\pi c}\right)^2 \frac{\exp(X_{\mathrm{so}})}{r a_{\mathrm{so}} [1 + \exp(X_{\mathrm{so}})]^2}, \tag{B12}$$

with $X_{\mathrm{so}} = (r - R_{\mathrm{so}})/a_{\mathrm{so}}$. The Becchetti and Greenlees parameters have the following values:

$$V_R = 54 - 0.32E + 24(N - Z)/A + 0.4Z/A^{1/3}, \tag{B13}$$

and

$$R_R = 1.17A^{1/3}, \qquad r_R = 0.75. \tag{B14}$$

The terms in V_R represent, respectively, the central potential, the energy term, the symmetry term, and the correction term for the Coulomb potential.

W_I is equal to $0.22E - 2.7$ or zero, whichever is greater; in this work the value of W_I is always zero. $W_{\rm der}$ is equal to $11.8 - 0.25E + 12(N - Z)/A$ or zero, whichever is greater, with $R_I = 1.32A^{1/3}$, $a_I = 0.51 + 0.7(N - Z)/A$, and $a_I = 0.477$. $V_{\rm so} = 6.2$, $R_{\rm so} = 1.01A^{1/3}$, and $a_{\rm so} = 0.75$.

The potential depth values and the beam energy E are in MeV, and the values of the radii R and diffuseness a are in fm. The Coulomb radius was chosen to be $R_c = 1.39(A^{1/3} + 1)$ fm. The values for V_R ($W_{\rm der}$) ranged from 54.28 (11.1) to 53.95 (10.84) over the energy range from 0.5 to 1.5 MeV (CM), and the calculations were made in steps of 0.01 MeV. The numerical integration of the radial wave functions in the HIOPTIM code is the very accurate Baylis-Peel algorithm [52], and integration was extended to 20 fm in steps of 0.025 fm; partial waves from $l = 0$ to $l = 3$ were used. The resulting phase shifts can be seen compared with hard-sphere phase shifts in Fig. 8.

[1] A. F. Iyudin *et al*., Astron. Astrophys. **300**, 422 (1995).
[2] A. F. Iyudin *et al*., *Proceedings of the Fourth INTEGRAL Workshop, 4–8 September 2001, Alicante, Spain*, ESA SP-459 (Noordwijk: ESA Publications Division, 2001), pp. 41–46.
[3] S. Starrfield *et al*., Phys. Rep. **227**, 223 (1993).
[4] URL http://astro.estec.esa.nl/Integral/about.html.
[5] C. Iliadis *et al*., Astrophys. J. Suppl. **142**, 105 (2002).
[6] J. José, A. Coc, and M. Hernanz, Astrophys. J. **520**, 347 (1999).
[7] C. Ruiz *et al*., Phys. Rev. C **65**, 042801 (2002).
[8] R. A. Paddock, Phys. Rev. C **5**, 485 (1971).
[9] A. B. McDonald and E. G. Adelberger, Nucl. Phys. **A144**, 593 (1970).
[10] C. Rolfs *et al*., Nucl. Phys. **A191**, 209 (1972).
[11] W. P. Alford *et al*., Nucl. Phys. **A457**, 317 (1986).
[12] S. Czajkowski *et al*., Nucl. Phys. **A616**, 278 (1997).
[13] B. Blank *et al*., Nucl. Phys. **A615**, 52 (1997).
[14] N. Bateman *et al*., Phys. Rev. C **63**, 035803 (2001).
[15] S. Michimasa *et al*., Eur. Phys. J. A **14**, 275 (2002).
[16] B. Davids *et al*., Phys. Rev. C **68**, 055805 (2003).
[17] J. Caggiano *et al*., Phys. Rev. C **66**, 015804 (2002).
[18] G. P. A. Berg *et al*., Nucl. Phys. **A718**, 608 (2003).
[19] A. Chen *et al*., Phys. Rev. C **63**, 065807 (2001).
[20] S. Bishop *et al*., Phys. Rev. Lett. **90**, 162501 (2003).
[21] J. Hardy, Phys. Rev. Lett. **91**, 082501 (2003).
[22] H. Grawe *et al*., Nucl. Phys. **A237**, 18 (1975).
[23] R. E. Laxdal, Nucl. Instrum. Meth. B **204**, 400 (2003).
[24] T. Delbar *et al*., Nucl. Phys. **A592**, 263 (1992).
[25] W. Galster *et al*., Phys. Rev. C **44**, 2776 (1991).
[26] J.-S. Graulich *et al*., Eur. Phys. J. A **13**, 221 (2002).
[27] J.-S. Graulich *et al*., Phys. Rev. C **63**, 011302 (2000).
[28] R. Coszach, Ph.D. thesis, Universite Catholique de Louvain, 1997.
[29] T. Davinson *et al*., Nucl. Instrum. Meth. A **454**, 350 (2000).
[30] D. J. Skyrme, Nucl. Instrum. Meth. **57**, 61 (1967).
[31] W. R. Leo, *Techniques for Nuclear and Particle Physics Experiments* (Springer-Verlag, Berlin, 1994).
[32] C. Ruiz, Ph.D. thesis, University of Edinburgh, 2003.
[33] B. Chambon *et al*., Phys. Rev. C **12**, 1 (1975).
[34] A. Anttila, Z. Phys. **234**, 455 (1970).
[35] J. Keinonen *et al*., Phys. Rev. C **15**, 579 (1977).
[36] H. L. Berg *et al*., Nucl. Phys. **A276**, 168 (1976).
[37] J. Görres *et al*., Nucl. Phys. **A385**, 57 (1982).
[38] J. Görres *et al*., Nucl. Phys. **A408**, 372 (1983).
[39] H. T. Fortune, R. Sherr, and B. A. Brown, Phys. Rev. C **68**, 035802 (2003).
[40] F. James, computer code MINUIT—Function Minimization and Error Analysis, CERN Program Library (Long Writeup D506) (2004), http://wwwasdoc.web.cern.ch/wwwasdoc/minuit/minmain.html.
[41] F. C. Barker, Aust. J. Phys. **25**, 341 (1972).
[42] C. Iliadis, Nucl. Phys. **A618**, 166 (1997).
[43] J. M. D'Auria *et al*., Phys. Rev. C **69**, 065803 (2004).
[44] P. Neogy *et al*., Phys. Rev. C **6**, 885 (1972).
[45] W. Scholz *et al*., Phys. Rev. C **6**, 893 (1972).
[46] A. M. Lane and R. G. Thomas, Rev. Mod. Phys. **30**, 257 (1958).
[47] E. Vogt, Rev. Mod. Phys. **34**, 723 (1962).
[48] E. Vogt (private communication).
[49] L. V. Namjoshi *et al*., Phys. Rev. C **13**, 915 (1976).
[50] N. M. Clarke, University of Birmingham, UK, 2003 (unpublished).
[51] F. D. Becchetti and G. W. Greenlees, Phys. Rev. **182**, 1190 (1969).
[52] W. E. Baylis and S. J. Peel, Comput. Phys. Commun. **25**, 7 (1982).